PD-(1+ PI) Controller for AGC of Power System based on Improved Grasshopper Optimization Algorithm

Pabitra Mohan Dash[a], Sangram Keshori Mohapatra[b], Asini Kumar Baliarsingh[c,], Dilip Kumar Bagal[d]*

[a]Department of Electrical Engg., BEC, Bhubaneswar, Odisha, India

[b]Department of Electrical Engg., GCE, Keonjhar, Odisha, India

[c]Department of Electrical Engg., GCE, Kalahandi, Odisha, India

[d]Department of Mechanical Engg., GCE, Kalahandi, Odisha, India

Abstract

In this article, the most recent technique for optimising structural components is discussed. This technique includes the Cascaded One Plus Proportional Integral (1+PI) controller with an Improved Grasshopper Optimization Algorithm-based Proportional Derivative (PD) controller for Automatic Generation Control (AGC) of the Power System. The thermal, hydro, and gas components, respectively, make up each individual control area. PID controllers are considered at the outset, and it has been shown that IGOA is more effective than Grasshopper Optimization Algorithm (GOA), Particle Swarm Optimization (PSO), and Genetic Algorithm (GA). The overshoots, undershoots, and other integral errors of frequency and tie-line power variances that occur after Step Load Perturbations (SLPs) are measured so that performance may be compared. Following that, PD cascaded with PI (PD-PI) and PD cascaded with One plus PI (PD-(1+PI)) controllers are considered, and IGOA approaches are used to improve controller settings. Finally, a Unified Power Flow Controller (UPFC) is investigated, and a comparison study is conducted using an IGOA tuned PD-(1+PI) controller in the presence of UPFC with PD-(1+PI) and PID controllers for various instances to demonstrate the superiority of the proposed controller.

Keywords: Automatic generation control; Cascade controller; Grasshopper Optimization Algorithm; PD-(1+ PI) controller;

1. Introduction

The power system is a form of electrical network known as a dispersed type, in which many control zones are linked with one another by tie-lines that are widely scattered across a huge territory. In order to meet the fundamental objectives of the power system, the ACE (Area Control Error) must be decreased as much as possible, and the generation control of each specific control area must be optimised with reference to the dynamically changing load demand that happens at various times of the day. The phenomenon of controlling the generation of energy according to the demand of customers is referred to as "AGC." According to (Kundur et al., 2022)'s study on dynamic loading circumstances, this control action preserves the frequency variations of the power system and the net exchange of the power across the tie-line at their goal values. The major purpose of automated gain control (AGC) is to decrease ACE while simultaneously protecting the system's stability. This is accomplished by ensuring that the performance parameter remains within the limit zone established by (Elgerd et al., 1971). (Elgerd and Fosha,1970) proposed the idea of a linked multi-area electric system, which was subsequently adopted by a large number of publications. The AGC of power systems has been optimised using a variety of different methodologies, and various researchers have

used a variety of control strategies. Cascaded controllers with different combinations are utilised for AGC. These combinations include PI-PD (Dash et al., 2014), PD-PID (Dash et al., 2015), two degrees of freedom (2DOF) plus PID (Sahu et al., 2013), Fuzzy Logic based PID Controller (Fuzzy PID) (Eftimie et al., 2007) and fuzzy logic PI controller (Sahu et al., 2015). (Zhou et al., 2020) developed a PD-type iterative learning control technique for a class of discrete spatially coupled systems with unstructured uncertainty. By lifting and altering the variable of discrete space model, the uncertain spatially linked systems is turned into equivalent single system, and the general state space model is produced in light of singular system theory. Then, the state error and output error information are utilised to create the iterative learning control rule, changing the controlled system into an analogous repeated process model. Based on the stability theory of repeating process, adequate condition for the stability of the system throughout the trial is provided in the form of linear matrix inequalities (LMIs) (Ezzat et al., 2021). It is necessary to have real-time structures that are based on more accurate and exact tools and have a high degree of swiftness competence as well as a high degree of accuracy and dependability in order to match the present rigorous quality criteria. Classical PID controllers are still preferred by engineers and researchers due to the user-friendliness of their features and the simplicity they provide in a variety of applications and in industrial automation. The proportional derivative, indicated by the notation "PD," with One Plus Proportional Integral (1+PI), is working in an acceptable way while achieving all of the design criteria (Sahu et al., 2019; Shayeghi et al., 2021). When undertaking a study of the steady state of an electric network, the main aim is to attain the lowest feasible steady-state error. It is required to make the integral controller gain bigger, yet doing so would create disruption in the performance. In order to preserve the dependability of the electric network's transient response, the steady-state error needs to be minimised as much as feasible by accurate actuation of the integrated controller in a range of dynamic states. With the assistance of a PD-1+PI) controller structure, this objective may be accomplished with relative ease. Controllers for Flexible AC Transmission Systems (FACTS) serve a crucial role in the process of managing the flow of electricity in a connected power system. In order to maximise the damping of oscillations, the Unified Power Flow Controller (UPFC), one of the most versatile FACTS controllers, may be connected in series or in a tie-line with the transmission line. When UPFC is present in the system, the components of that component should operate together in a coordinated fashion so that they may regulate the circumstances of the network in a very quick and cost-effective way (Narain et al., 2000).

According to the results of a prior literature review on AGC, the performance of an electric power network is reliant on the controller techniques and the optimization methodology for the tuning of controller gains. As a consequence of examining the aforementioned literature, this was found. Some conventional controllers, such as PID, Fuzzy PID, optimal control, cascaded PID controller, 2DoF controller, Integral Double Derivative (IDD) controller, etc., in conjunction with some optimization techniques, such as Differential Evolution (DE) (Mohanty et al., 2014; Jiang et al., 2022), Particle swarm optimization (PSO) (Prasad et al., 2015; Khokhar et al., 2021), 'Artificial bee colony (ABC)' (Naidu et al., 2014), Cuckoo search (CS) (Dash et al., 2016), and Teaching Learning In addition, several publications use other metaheuristic techniques, such as the Symbiotic Organism Search (SOS) (Barisal, 2015), the Bat Algorithm (Kaliannan et al., 2019) the Whale Optimization Algorithm (WOA) (Abd-Elazim and Ali, 2016), and the Grey Wolf Optimization (GWO) (Nayak et al., 2018), among others. In several works, it has been found that classical controller methods or classical optimization approaches, or potentially all metaheuristic optimization

techniques, are unable to effectively offer optimum solutions that are adequate for multi-objective power system problems in global space. This has been the case for quite some time. The "No Free Lunch" (NFL) theorem states that it has been rationally shown that there is no such optimization approach available that is capable of solving all different kinds of issues. Recently, improved/modified optimization approaches have been applied for many controller design problems for frequency control. An improved Grey Wolf Optimization (GWO) based fractional ordered type-II fuzzy controller for frequency awareness of an AC microgrid under plug in electric vehicle has been presented in (Nayak et al., 2018). A Quasi oppositional Jaya tuned two-degree of freedom PID has been projected of a two area system including the nonlinearities in (Guha et al., 2022). A sine logistic map based chaotic sine cosine algorithm tuned PID for frequency regulation of a microgrid with PV, wind, Fuel Cell, BESS, FESS, DEG and MT (Sahu et al., 2021). A 2DOF-tilted integral derivative with filter tuned by bat and harmony search algorithm has been proposed for two-area wind-hydro-diesel units with SMES and FACTS devices (Peddakapu et al., 2021). In (Abou et al., 2022), a PDF-PI structure tuned by coyote optimization was suggested for frequency regulation of a two-area power system with PV, wind farm & gas turbine interconnection. A Chaotic atom search optimization tuned FOPID structure for frequency control of a hybrid system was presented in (Irudayaraj et al., 2022). Mayfly optimization tuned Fuzzy PD-(1+I) configuration was recommended in (Sahu et al., 2015) for a microgrid containing Solar–thermal, Wind, Micro-hydro turbine, Biodiesel and Biogas generators. A simplified GWO based adaptive fuzzy PID controller has been proposed to control frequency of hybrid power system containing PEV, WTPG, STPG and thermal units considering nonlinearities (Padhy and Panda, 2021). Recent research by (Saremi et al., 2017) has suggested a method that takes its cues for success from the cooperative behavior of grasshoppers. The Grasshopper Optimization Algorithm (GOA) was the name that was given to the method. These days, algorithms that are inspired by nature are used rather often because of their ease of implementation, the ability to avoid reaching a high local optimum value, and the presence of a gradient-free mechanism. Therefore, the effectiveness of using the proposed strategy to address real-world issues is being evaluated. The answers have to be improved using algorithms that are inspired by nature until the final requirement is satisfied. In addition to this, exploration and exploitation are the respective names for the two steps of the optimization process. Exploration refers to the algorithm's tendency to display overly random behaviour in order to dramatically modify the findings. Large variances in the answers lead to further study of the search space, which then leads to the finding of the space's promising regions. However, since algorithms have a tendency to exploit opportunities, solutions often come across smaller-scale changes and have a tendency to seek out solutions in a localised area. The search for the global optimum solution to a particular optimization problem may be accelerated by finding a balance between exploration and exploitation of a resource. According to (Mohanty and Panda, 2021), the Gravitational Search Algorithm (GSA), the State of Matter Search (SMS), the Firefly Algorithm (FA), the Bat Algorithm (BA), the Flower Pollination Algorithm (FPA), the Gravitational Search Algorithm (GSA), and the General Algorithm (GA) all produce inferior results compared to the Gravitational Optimization Algorithm (GOA), which generates superior results. The performance of the original GOA in calculating the zone of attraction, zone of repulsion, and zone of comfort is greatly reliant on selecting the coefficient 'c' appropriately. This parameter is progressively lowered from 1 all the way down to 0.000001 in the original GOA. An enhanced version of GOA known as IGOA has been suggested as a result of this research. In

IGOA, the value of the parameter c is changed in such a way as to result in an improvement in the performance of the algorithm.

Taking into consideration the aforementioned characteristics, a two-control area model was developed, and it is composed of gas units, thermal power units, and hydro power units. The suggested IGOA-based PD-(1+PI) controller is offered for the aim of obtaining AGC for the investigated system. In order to demonstrate the advantages of the recommended controller, the IGOA-tuned PD-(1+PI) controller compares UPFC with PID and PD-(1+PI) controller in various situations. The following is a summary of the article's most crucial points:

- A revised version of the GOA is suggested, and it is compared to the GA, the PSO, and the GOA.
- A comparison study comparing overshoots, undershoots, and various integral errors of frequency and tie-line power fluctuations following Step Load Perturbations (SLPs) in each site has been done. This research examined both overshoots and undershoots.
- A PD-(1+PI) controller structure is predicted to act as the controller for the automated generation control of a multisource power network.
- The IGOA method is used to modify the PD-(1+PI) controller gains in the presence of UPFC, and the results are compared with those achieved using PID and PD-(1+PI) structures for the different situations.

2. System under study

As illustrated in Fig. 1, the simulation prototype contains two control regions and an electric network that pulls power from many sources. Each area has its own unique mix of thermal power plants, hydropower plants, and gas power plants. The work by (Padhan et al., 2014) that was utilised as a reference for the transfer function model of the conventional power source hydro power unit and thermal power unit has been cited. This article by (Sahu et al., 2019) cites the transfer function model of the gas generator unit (Irudayaraj et al., 2022).

2.1 Mathematical Modeling of Components

2.1.1 Modelling of Thermal Power Plant

The thermal power system is comprised of numerous components, including the generator, governor, turbine, and reheater. In order to depict these components accurately, the following transfer function has been chosen (Padhan et al., 2014):

$$G_p(s)= \frac{K_p}{1+sT_p} \quad (1)$$

$$G_g(s)= \frac{K_g}{1+sT_g} \quad (2)$$

$$G_t(s)= \frac{K_t}{1+sT_t} \quad (3)$$

$$G_r(s)= \frac{1+sK_rT_r}{1+sT_r} \quad (4)$$

2.1.2 Modelling of Hydro Power Plant

The mentioned equation describes the transfer function of the hydropower plant's mechanical "hydraulic governor" and "hydro turbine" (Irudayaraj et al., 2022):

$$G_{HG}(s)= \left[\frac{K_1}{1+sT_1}\right]\left[\frac{1+sT_R}{1+sT_2}\right] \quad (5)$$

$$G_r(s)= \frac{1+sT_W}{1+0.5*sT_W} \quad (6)$$

where, T_1, T_R, T_2, and $T_W$represent the 'hydro plant's speed governor, "reset time, "main servo time constant,' and 'nominal beginning time of water in hydro plant penstock', respectively. Modelling and simulating complex systems, such as forestry equipment, are frequently the only approach for their comprehensive study and design. Two different techniques are studied by Nedić et al. in two ways. The first one relates to the use of a variable step of integration by continuous models suited to the quickest processes. The second one deals to the approximation of rapid transitions using ideal instantaneous mode-transitions and hybrid models (Nedić et al., 2017).

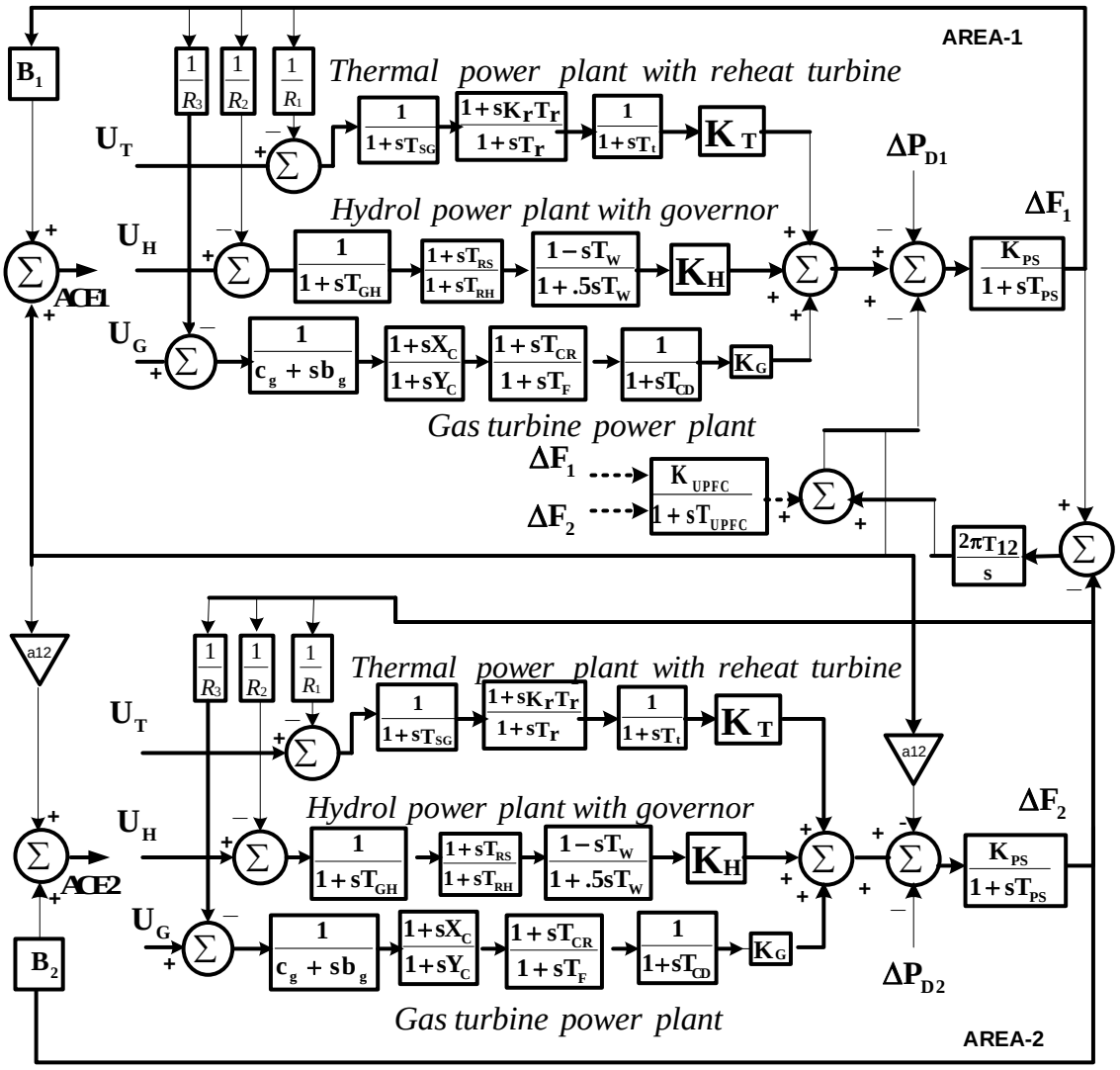

Fig. 1 Two area multi source system under study

2.1.3 Modelling of Gas Power Plant

Typically, a gas turbine power plant will consist of the valve positioner, speed governor, fuel system, combustor, and gas turbine. Fig. 1 depicts the transfer function employed by the valve positioner, where cg is the gas turbine valve positioner and bg is the gas turbine constant for the valve positioner. The lead-lag compensator, which is a depiction of the speed regulating mechanism, is shown in Fig. 1, where XC represents the lead time

constant of the gas turbine speed governor in seconds and YC represents the lag time constant of the gas turbine speed governor in seconds. Fig. 1 depicts the fuel system and combustor as a transfer function with the pertinent time constants, where TF is the gas turbine fuel time constant in seconds and TCR is the gas turbine combustion response delay in seconds. A transfer function for a gas turbine consists of a single time constant known as the gas turbine compressor discharge volume-time constant (TCD) in seconds.

2.1.4 Modelling of UPFC

The Unified Power Flow Controller (UPFC) is regarded as one of the most versatile devices in the FACTS family of devices owing to its ability to regulate the flow of power in the transmission line, improve transient stability, reduce system oscillation, and provide voltage support (Guha et al., 2022). In this study, the two-area power system that contains a UPFC and is shown in Fig. 2 is examined.

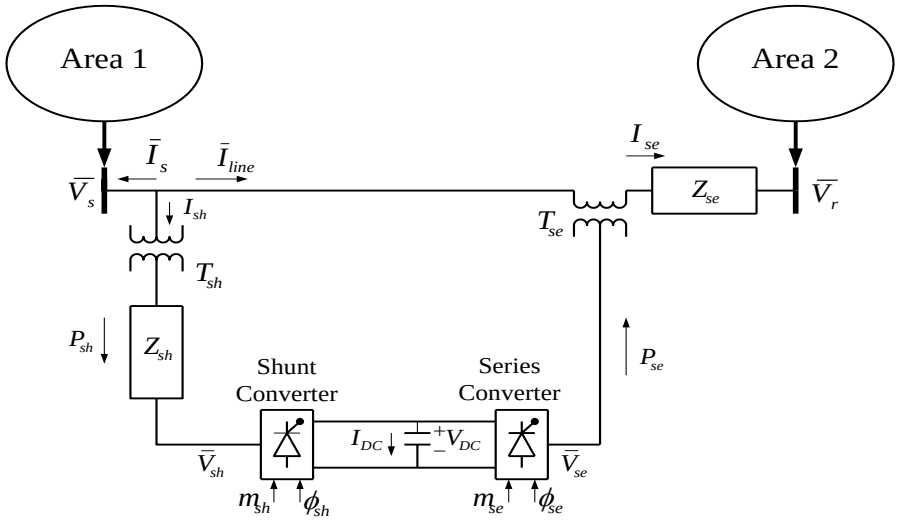

Fig. 2 Two area interconnected power system with UPFC

The UPFC is linked in series with a tie-line to attenuate oscillations in the tie-power line's supply. In Fig. 2, V_{se} represents the magnitude of the series voltage, and ϕ_{se} represents the phase angle of the series voltage. The shunt converter will inject a regulated shunt voltage into the circuit such that the actual component of the current that is flowing through the shunt branch will be in equilibrium with the real power that is being required by the series converter. It is plainly clear from Fig. 2 that the complex power at the receiving end of the line is computed as follows:

$$P_{real} - jQ_{reactive} = \overline{V_r^*} I_{line} = \overline{V_r^*} \left\{ \frac{(\overline{V_s} + \overline{V_{se}} - \overline{V_r})}{j(X)} \right\} \tag{7}$$

where $\overline{V_{se}} = |V_{se}| \angle(\delta_s - \phi_{se})$ (8)

Solving the equation (1), the real part as given below

$$P_{real} = \frac{|V_s||V_r|}{(X)} \sin(\delta) + \frac{|V_s||V_{se}|}{(X)} \sin(\delta - \phi_{se}) = P_0(\delta) + P_{se}(\delta, \phi_{se}) \tag{9}$$

If V_{se} is equal to zero in the equation above, it indicates that the system's actual power is uncompensated. In contrast, the amplitude of the UPFC series voltage may be set anywhere between 0 and V_{se} max, and its phase angle (ϕ_{se})

which is adjustable from 0 to 360^0at any power angle. AGC permits the following UPFC-based controller representations:

$$\Delta P_{UPFC}(s) = \left\{\frac{1}{1+sT_{UPFC}}\right\}\Delta F(s) \tag{10}$$

where T_{UPFC} is the time constant of UPFC.

3. Proposed Approach

3.1 Controller Structure

Due to its versatility, PID controllers are used in a number of scenarios throughout this article along with simplicity, efficiency, and resilience. The following is the generalised expression for a PID controller written down in the form of a transfer function:

$$Tf_{PID} = K_P + \frac{K_I}{s} + K_D s \tag{11}$$

Examining the steady state of the transient response reveals that the PID controller cannot provide optimal results in a number of situations. On the other hand, integral gain reduces steady-state error, but this results in oscillations with dynamic behaviour. The speed of the response is slowed down during the transient stage by the integral gain, which also decreases the steady-state stability. It is common practise to disable the integral parameters in order to get improvements in the transient response. Using a PD-(1+ PI) controller makes this straightforwardly doable. It consists of two phases: a filter-linked PD controller in the first half, followed by a PI controller in the second. This enables it to maintain reaction speed by overcoming steady-state error, and it gives system stability. Cascade PD-(1+ PI) controllers were chosen to tackle the AGC issue in this research in light of the previously mentioned considerations. Fig. 3 depicts the construction of a PD-(1+ PI) controller in its entirety.

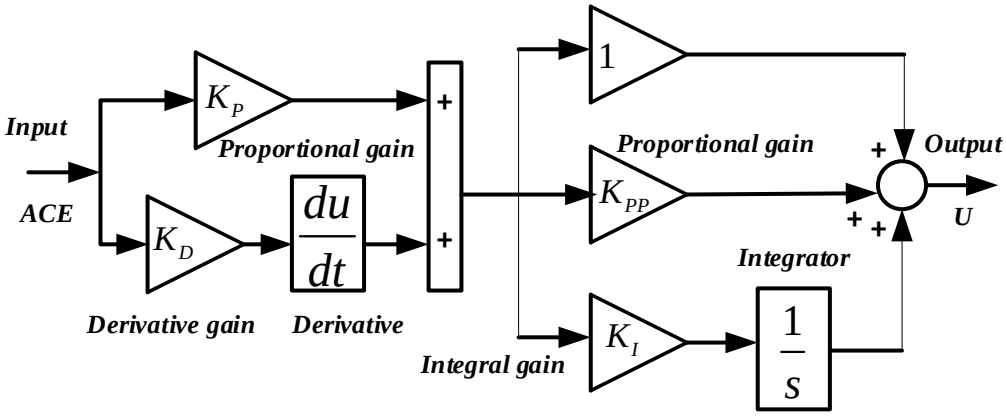

Fig. 3 Structure of PD-(1+ PI) controller

The transfer function of the PD-(1+ PI) controller may be expressed as follows:

$$TF_{PD-(1+PI)} = (K_{P+}K_D s)(1 + K_{PP+}K_I/s) \tag{12}$$

Where K_P, K_I, K_D,and K_{PP}represent the proportional-gain, integral-gain, derivative-gain, and second-stage proportional-gain respectively, in Fig. 2 of the PD-(1+ PI) control model. The Area Control Error (ACE) is supplied as an input to the PD-(1+ PI) controller, and the controller's output is provided as an input to the power system. The ACE is calculated by linearly factoring in the errors in the system frequency and the tie-line power, which may be stated as follows:

$$\mathrm{ACE}_i = \beta_i \Delta F_i + \sum_{\substack{j=1 \\ j \neq i}}^{n} \Delta P_{ij} \tag{13}$$

3.2 Objective function

It is essential to make an objective function selection that is appropriate for the system performance goals that are being pursued. When the aim is to decrease both the frequency deviation (ΔFi) and the control efforts (ΔU), the integral square error (ISE) is viewed as an objective function.

$$J = \int_0^t \left[k_n w \left((\Delta F_i)^2 + (\Delta P_{tie\,i-j})^2 \right) + (1-w)(\Delta U)^2 \right] dt \tag{14}$$

Where "*t"* is the duration of the simulation. In order to ensure that both of the components in Equation (14) are competitive in the search technique, the values 500 and 0.5 have been set to k_n and w, respectively.

The objective function is minimised in order to pick the controller gains while adhering to the limitations imposed by $K_{P\,Min} \leq K_p \leq K_{P\,Max}$, $K_{D\,Min} \leq K_D \leq K_{D\,Max}$, $K_{I\,Min} \leq K_I \leq K_{I\,Max}$, $K_{PPMin} \leq K_{pp} \leq K_{PP\,Max}$. The maximum and minimum values of the associated controller parameters are denoted by the subscripts Max and Min, respectively.

Various integral-based objective functions, such as IAE, ISE, ITAE, ITSE, and ISTAE, are used to evaluate the system's performance. These functions' specifics are as follows:

$$J_1 = ISE = \int_0^T \left((\Delta F_i)^2 + \left(\Delta P_{tie\,i-j} \right)^2 \right) dt \tag{15}$$

$$J_2 = ITSE = \int_0^T \left((\Delta F_i)^2 + \left(\Delta P_{tie\,i-j} \right)^2 \right) t\, dt \tag{16}$$

$$J_3 = IAE = \int_0^T \left(|\Delta F_i| + \left| \Delta P_{tie\,i-j} \right| \right) dt \tag{17}$$

$$J_4 = ITAE = \int_0^T \left(|\Delta F_i| + \left| \Delta P_{tie\,i-j} \right| \right) t\, dt \tag{18}$$

$$J_5 = ISTAE = \int_0^T \left(|\Delta F_i| + \left| \Delta P_{tie\,i-j} \right| \right) t^2\, dt \tag{19}$$

Where ΔF_i = frequency deviation i^{th} area, $\Delta P_{tie\,i-j}$= tie-line power deviation among i^{th} and jth area and T = time of simulation.

4. Overview of GOA and its Improvement

GOA is the name of a strategy recently proposed by (Saremi et al., 2017) that draws inspiration from nature. This method is based on the social activities of grasshoppers. Grasshoppers are constantly searching for food, which requires them to engage in actions such as exploration and exploitation. Therefore, the behavior of grasshoppers may serve as a basis for the development of a mathematical model. The following is the mathematical model that has been offered for the swarming behavior of grasshoppers:

$$X_i = S_i + F_i + W_i \tag{20}$$

Where, the location of the ith grasshopper denoted by the letter X_i, similarly S_i stands for social interaction, F_i denotes the force due to gravity of ith grasshopper and lastly, W_i represents wind advection. It is important to keep in mind that the aforementioned condition may be put together in such a way as to create highly randomized behavior as $X_i = r_1 I_i + r_2 F_i + r_3 W_i$ where r_1, r_2 and r_3 are highly randomized value in the range of [0,1].

$$S_i = \sum_{\substack{l=1 \\ l \neq k}}^{N} s(d_{kl}).\hat{d}_{kl} \tag{21}$$

where, d_{kl} is the distance that must be travelled between the grasshoppers k and l, and it may be computed as $d_{kl} = \left| X_l - X_k \right|$ and the value of s quantifies the intensity of the social interaction forces, and $\hat{d}_{kl} = \frac{X_l - X_k}{d_{kl}}$ is a unit vector between the k^{th} and i^{th} grasshoppers.

The so-called social interaction forces are denoted by the letter "s," and they are computed as:

$$s(r) = ae^{-\frac{r}{l}} - e^{-r} \tag{22}$$

where l represents the attractive length scale and a represents the attractive force between the two objects.

This function represents the impacts on grasshopper community interaction, with the range of this function ranging from 0 to 15 (Sahu et al., 2018). This is when the repulsive effect takes place [0 2.079]. There is no attraction nor repulsion between two grasshoppers separated by 2.079 units. It is often referred to as the safe distance or the comfort zone. According to the findings (Zhou et al., 2020), the intensity of the attraction steadily rises from 2.079 to 4 distance units before continuing to gradually decrease after reaching this threshold. Changing the parameters l and a in Equation (22) leads the artificial grasshoppers to participate in a variety of social behaviors. Despite the fact that the function may divide the area inhabited by two grasshoppers into an attraction region, a repulsion region, and a comfort zone, for separations greater than 10, this function returns a value near to zero. Therefore, in the event that there is a significant amount of space between the grasshoppers, this function will be unable to exert any pressure between them. In the meantime, between [1, 4], a separation of grasshoppers is being mapped out in order to identify this difficulty. The F component of Equation (20) may be found by using the formula:

$$F_i = -g\hat{e}_g \tag{23}$$

where g refers to the gravitational constant and $\hat{e}_g$ is the unit vector to the centre of the Earth.

It is predicted that the component W_i in Equation (20) is as:

$$W_i = u\hat{e}_w \tag{24}$$

where *u* stands for the drift constant and $\hat{e}_w$ denotes the direction of the wind's unity vector.

Since grasshopper nymphs do not yet have wings, their movement is mostly determined by the direction in which the wind is blowing. This equation may be expanded further by replacing the *S*, *F*, and *W*,in Equation (22), resulting in the following:

$$X_i = \sum_{\substack{l=1 \\ l \neq k}}^{N} s\left(\left| X_l - X_k \right|\right) \frac{X_l - X_k}{d_{kl}} - g\hat{e}_g + u\hat{e}_w \tag{25}$$

Where, the number of grasshoppers is denoted by the letter *N*.

Since nymph grasshoppers land on the ground, their position must remain above a certain threshold value at all times. Therefore, in order to replicate the interaction between grasshoppers in a swarm, Equation (25) is applied. In

order to address the optimization issues, the GOA takes into account the following updated version of the equation that was previously presented.

$$X_i^d = c\left(\sum_{\substack{l=1 \\ l\neq k}}^{N} c\frac{ub_d - lb_d}{2} S\left(\left|X_l^d - X_k^d\right|\right)\frac{X_l - X_k}{d_{kl}}\right) + T_d \quad (26)$$

where ub_d is the upper bound and lb_d is the lower bound in the dimension *D-th*, T_d is the target value and c is a diminishing coefficient that reduces the size of the zone of comfort, zone of repulsion, and zone of attraction. It is essential to note that S approximately corresponds to the S component of the equation (21). In this equation (26), gravity is ignored and it is assumed that the wind always blows in the target's direction.

The value of the parameter c in Equation (26) describes the pace at which the grasshopper slows as it approaches the food source and as it consumes it. Both components of Equation (25) are multiplied by random variables in order to quantify the level of unpredictability inherent in grasshopper interactions. Before exploiting and exploring the search space, mathematical formulations must be accounted for. In addition, a search agent is required to regulate the quantity of exploitation and exploration. As grasshopper nymphs lack wings, they must search for food in close proximity to their environment. When they reach adulthood, they explore a huge search space region. Exploration happens first in this strategy, just as it does in stochastic optimization. The primary effort is first placed on locating potentially fruitful search spaces. Following exploration, exploitation is the process of looking for food in potentially fruitful places locally in order to achieve the highest possible value on a worldwide scale. The behavior of the grasshopper has been significantly shaped by c to a considerable extent, and the number of iterations keeps growing. Lower "*c*" values reduce the attraction or repulsion forces between grasshoppers, but higher "*c*" values reduce the search space around the objective maximum.

Following is the formula for determining the decreasing coefficient '*c*':

$$c = c_m - I\frac{c_m - c_n}{L} \quad (27)$$

where c_m and c_n represent the absolute maximum value and absolute lowest value respectively, I represents the present iteration and L stands for the highest iterations amount. In the first iteration of the GOA algorithm, c_m and c_n were assigned the values 1 and 0.00001 respectively.

The value of the coefficient denoted by the letter "c" in Equation (26), which is implemented in GOA, has a significant bearing on the degree to which the algorithm converges. Because it has a smaller value, c causes a more gradual approach to the aim, which acts as the point of convergence. As a consequence of this, the algorithm will work to prevent itself from being mired in a local optimum, thus raising the likelihood that it will eventually arrive at the value that represents the global optimum. In the original GOA, the value of 'c' is decreased in a linear fashion from 1 to 0.00001; however, in the method that has been suggested, the coefficient c is decreased from 1 to 0.00001 in such a way that it is lowered gradually at the beginning and quickly towards the conclusion of the iteration. This is done in order to achieve the best possible results. This slow change in c value will lead to an increase in the algorithm's capacity for exploratory behavior, which is something that will be to the algorithm's advantage. A

correction factor of 1.5 is used in IGOA to calculate both the current iteration, which is marked by the letter I, and the maximum number of iterations, which is denoted by the letter L. The accuracy of this adjustment factor is determined by a process of several test runs. Therefore, the answer to Equation (27) should be rewritten as shown in Equation (below) (28).

$$c = c_m - I^{1.5}\left(\frac{\left(c_m - c_n\right)}{L^{1.5}}\right) \tag{28}$$

5. Results and Discussions

Studies are now being conducted to assess the efficacy of the technique that was proposed before for frequency modulation of the two-area multi-source system that is shown in Fig. 1. In area-1, it is anticipated that there would be a load disturbance of 1 percent (PD1 = 0.01), and in area-2, it is estimated that there will be a load disturbance of 3 percent (PD2 = 0.03). In the beginning, PID controllers are taken into consideration, and UPFC is left out of the system altogether. This is done so that the better performance of the IGOA approach can be verified. IGOA, GOA, PSO, and GA are the optimization methods that are used on the controller parameters. The appendix contains the many parameters that are used by these methods. [-2, 2] has been decided upon as the appropriate range for the controller's settings. Consideration is given to 30 different search agents and 100 different iterations across all of the algorithms. All of the techniques that have been described are carried out a total of thirty times, and the best values for the controller gains are chosen based on the least J value that is provided by equation (14). The compared algorithm parameters are given in Table 1. The GA, PSO and GOA parameters are taken from reference (Saremi et al., 2017). The minimum, maximum, average and standard deviation values obtained in 30 runs are gathered in Table 2 from which it is clear that IGOA outperforms GA, PSO and GOA methods. Table 3 has a listing of all of the optimized parameters as per minimum *J* value. The convergence curves corresponding to the best results for each algorithm is given in Fig. 4 from which it is clear that, IGOA converges faster with improved results than others.

Table 1 Parameter setting of different algorithms

Method	Parameter	Description
GA	Selection	Roulette wheel
	Crossover	Single point (probability = 1)
	Mutation	Uniform (probability = 0.01)
PSO	Inertia weight, w	Reduces from 0.6 to 0.3
	Social & Cognitive components, c_1 &c_2	1.5, 1.5
GOA	Parameter '*c*'	$c = c_m - I\frac{c_m - c_n}{L}$
	c_m and c_n	1 and 0.00001
	Parameter '*l*' and '*f*'	1.5 and 0.5
IGOA	Parameter '*c*'	$c = c_m - I^{1.5}\left(\frac{\left(c_m - c_n\right)}{L^{1.5}}\right)$
	c_m and c_n	1 and 0.00001
	Parameter '*l*' and '*f*'	1.5 and 0.5

Table 2: Statical outcome of 30 independent runs

Technique/ Controller	J_{MIN}	J_{MAX}	J_{AVE}	J_{STD}
GA	9.0546	12.7062	10.2461	2.1215
PSO	7.5140	10.615	9.7193	1.8721
GOA	6.4677	9.3316	7.8519	1.5241
IGOA	4.9302	6.4463	5. 5728	1.1472

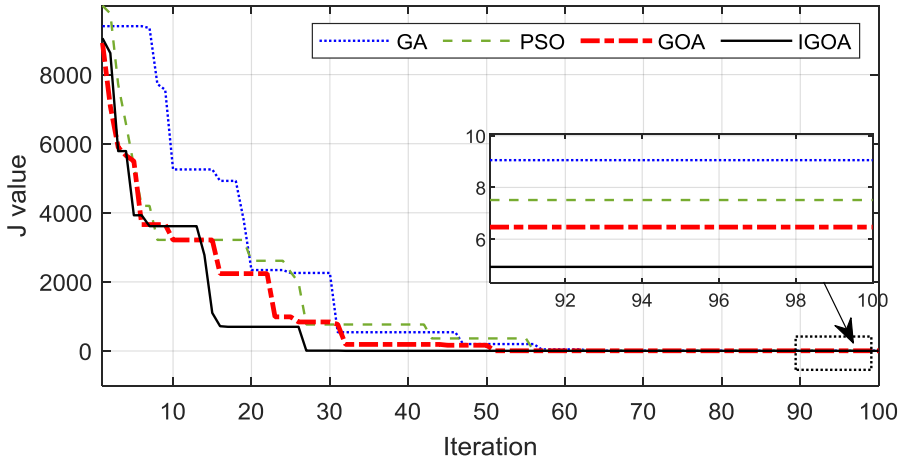

Fig. 4 Comparison of convergence curves

Table 3: Optimal PID controller parameters

Unit/Parameters		Area-1			Area-2			*J* Value
		Thermal	Hydro	Gas	Thermal	Hydro	Gas	
GA	K_P	-1.7319	1.9138	0.5153	0.6247	-0.6857	-0.0968	9.0546
	K_I	-0.9640	-1.1995	1.4834	-1.8855	-1.8490	-0.2464	
	K_D	-1.9292	-1.1959	1.4314	-1.7245	-0.7541	1.3042	
PSO	K_P	-1.9893	1.4984	0.5211	0.4070	-0.6614	-0.0958	7.5140
	K_I	-0.9860	-1.1930	0.9235	1.6590	-1.2033	-0.2360	
	K_D	-1.8327	-1.1569	1.3734	-1.6240	-0.5537	0.9582	
GOA	K_P	-2.0137	1.4513	0.4432	0.3118	-0.5578	-0.0857	6.4677
	K_I	-1.0897	-1.0172	1.049	1.6551	-0.9821	-0.2550	
	K_D	-1.8389	-1.3240	1.1439	-1.7098	-0.6116;	0.8996	
IGOA	K_P	-1.6485	1.7041	-1.4016	-1.3537	0.8697	0.6988	4.9302
	K_I	-0.2409	-0.769	-0.8967	-1.4404	-1.3295	-0.0231	
	K_D	-0.5635	-1.6331	-1.9611	-0.5066	1.1513	-0.2093	

According to Table 3, it is abundantly obvious that when using PID, the *J* value achieved with GOA is much lower than that obtained with GA and PSO. When IGOA is used, the *J* value is lowered by an even greater amount. In comparison to GA, PSO, and GOA, the percentage decrease in *J* value that may be achieved with the IGOA approach that has been presented is 45.55 percent, 34.38 percent, and 23.77 percent, respectively.

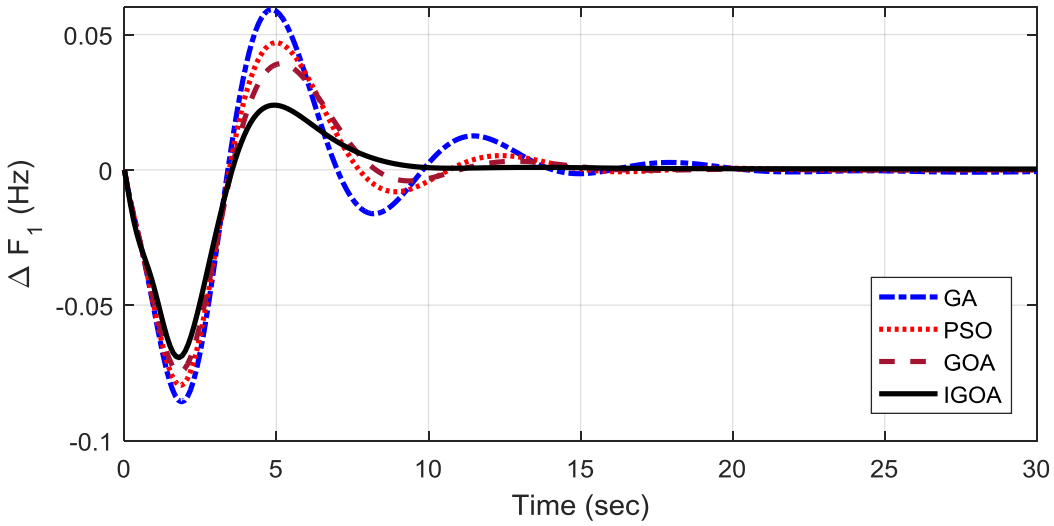

(a) ΔF_1

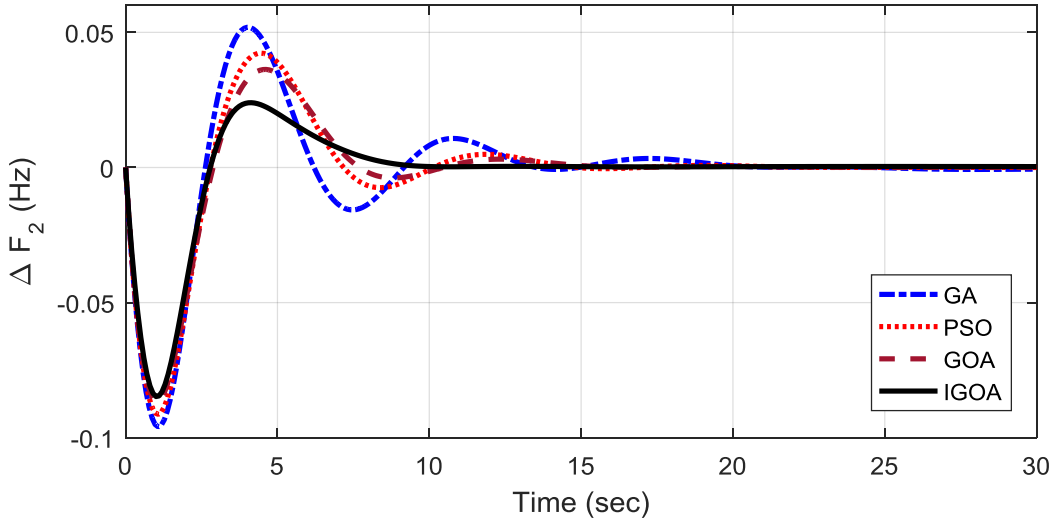

(b) ΔF_2

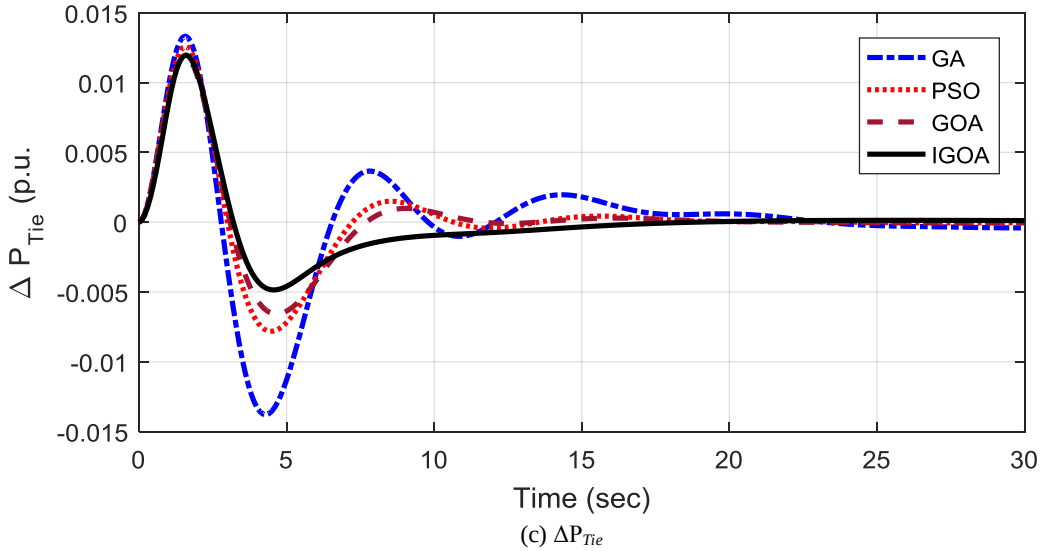

(c) ΔP_{Tie}

Fig. 5 System response showing comparison of techniques

Figs. 5 (a)-(c) show the system's reaction to the perturbation described above. Figs. 5 (a)-(c) show that the IGOA method outperforms the GA, PSO, and GOA approaches in terms of transient performance when used in conjunction with the same PID controller.

The comparative report of transient characteristics using different integral errors, maximum overshoot (MOs), and maximum undershoot (MUs), of ΔF_1, ΔF_2, ΔP_{Tie} of the proposed system with PID controller optimized by above techniques are given in Table 4. It is evident from this table that the IGOA optimised PID controller produces the least mathematical value integral errors in comparison to the GA, PSO, and GOA optimised PID controllers. This confirms the superiority of IGOA technique over GA, PSO and GOA techniques in studied controller design problem. (Sulaiman et al., 2019) compared IGOA approach with Grasshopper Optimization Algorithm (GOA), Genetic Algorithms (GA), Evolutionary Strategy Optimisation (ESO), Differential Evolution (DE), Particle Swarm Optimization (PSO), Harmony Search (HS) and Hybrid Harmony Search (HHS). And, they found that IGOA has the better results in terms of convergence rate and quality of solutions for solving economic load dispatch problems. In terms of Convergence rate, Jiang et al. addressed the learning-based adaptive optimum output regulation issue with convergence rate requirement for disturbed linear continuous-time systems. An adaptive optimum control strategy is suggested based on reinforcement learning and adaptive dynamic programming to learn the optimal regulator with ensured convergence rate (Jiang et al., 2022).

Table 4: Performance comparison of different techniques

Controller/ Technique	Integral errors					Max. Overshoots (MO_S)			Max. Undershoots (MU_s) (-ve)		
	ISE	ITAE	ITSE	IAE	ISTAE	ΔF_1	ΔF_2	ΔP_{Tie}	ΔF_1	ΔF_2	ΔP_{Tie}
GA	0.0355	4.3593	0.0981	0.8087	56.7214	0.0592	0.0519	0.0133	0.0857	0.0960	0.0138
PSO	0.0296	2.6602	0.0742	0.6640	21.0294	0.0470	0.0423	0.0126	0.0796	0.0914	0.0078
GOA	0.0254	2.2591	0.0606	0.5983	17.1537	0.0392	0.0363	0.0119	0.0747	0.0866	0.0066
IGOA	0.0192	2.0802	0.0366	0.4994	16.7201	0.0239	0.0240	0.0120	0.0694	0.0848	0.0049

The following step involves using the IGOA approach in order to optimise the PD-PI and PD-(1+PI) controllers, both with and without UPFC. Table 5 presents the parameters after they have been optimised. According to Table 5, it is abundantly evident that when using PID, obtaining a *J* value with PD-(1+PI) results in a lower value than when using PID and PD-PI. When UPFC is implemented, the *J* value drops much lower than it was before. When compared to PD-PI and PID, the percentage reduction in *J* value achieved by using PD-(1+PI) is 60.37 percent, while PD-PI and PID only achieve 45.16 percent. With UPFC the *J* value is further reduced by 40.36% compared to without UPFC.

Time-domain simulations of the following instances are taken into consideration for the purpose of comparing and assessing the performance of the system.

Case 1: SLPs in each area

Case 2: Change in SLPs in each area.

Case 3: Change in SLPs in each area with uncertainty in system parameter

Table 5: Optimal controller parameters

Unit/Parameters		Area-1			Area-2			*J* Value
		Thermal	Hydro	Gas	Thermal	Hydro	Gas	
PD-PI	K_P	0.8053	-0.1079	1.3332	-1.5199	0.8568	1.3184	3.5630
	K_I	-1.3448	-0.3563	0.3690	0.2523	0.1945	-1.7785	
	K_D	0.9444	0.6623	-1.0438	-1.5735	0.7458	-0.9637	
	K_{PP}	-1.2641	0.9649	1.2302	0.8848	0.5750	-1.1007	
PD-(1+PI)	K_P	-0.4746	0.5860	-0.6413	-1.6224	0.5902	0.0609	1.9538
	K_I	0.7271	-0.6942	1.6710	1.5099	0.4483	1.4483	
	K_D	-0.5497	-0.2188	0.5751	-1.6078	0.7005	-0.1762	
	K_{PP}	0.6877	1.0618	0.7905	-0.0085	1.4592	-1.1103	
PD-(1+PI) with UPFC	K_P	-1.9890	1.5928	1.7005	-1.6545	-0.1042	0.6356	1.1651
	K_I	0.5595	0.0543	-0.6203	0.4612	-1.4431	-1.6981	
	K_D	-0.7786	0.9062	0.1964	-0.2558	-0.7806	0.8386	
	K_{PP}	1.2158	0.8720	-0.3607	1.9688	-0.6854	0.1137	

Case 1:

In this specific situation, both a 1 percent load disturbance in area-1 (PD1=0.01) and a 3 percent load disturbance in area-2 (PD2=0.03) are taken into account. Fig. 6 depicts these several rounds (a). The dynamic responses of the IGOA-optimized PID, PD-PI, PD-(1+PI), and PD-(1+PI with UPFC are displayed in Figs. 6 (a)-(c), respectively. As shown in Figs. 6 (a)-(c), the transient performance of the PD-(1+PI) controller is superior to that of the PID and PD-PI controllers in terms of low errors and MUs/MOs compared to the performance of other controllers (c). When UPFC is taken into account, performance improves even more. The comparison report of transient characteristics of various integral errors, maximum overshoot (MOs) and maximum undershoot (MUs), of ΔF_1, ΔF_2, ΔP_{Tie} of the proposed system for Case 1 is given in Table 6. This table demonstrates that the mathematical values J, integral errors, MOs, and MUs attributed to PD-(1+PI) with UPFC are the lowest when compared to alternative methods. Fig. 7 shows the input and output control signals of the proposed model.

Table 6: Performance comparison of IGOA optimized controllers for Case-1

Controller/ Technique	Integral errors					Max. Overshoots (MO_S)			Max. Undershoots (MU_s) (-ve)		
	ISE	ITAE	ITSE	IAE	ISTAE	ΔF_1	ΔF_2	ΔP_{Tie}	ΔF_1	ΔF_2	ΔP_{Tie}
PD-PI	0.0134	1.0370	0.0210	0.3587	6.1421	0.0114	0.0102	0.0093	0.0621	0.0724	0.0007
PD-(1+PI)	0.0075	0.9276	0.0117	0.2829	6.3472	0.0091	0.0101	0.0032	0.0510	0.0486	0.0012
PD-(1+PI) with UPFC	0.0043	0.4035	0.0049	0.1884	2.1326	0	0.0006	0.0080	0.0387	0.0425	0

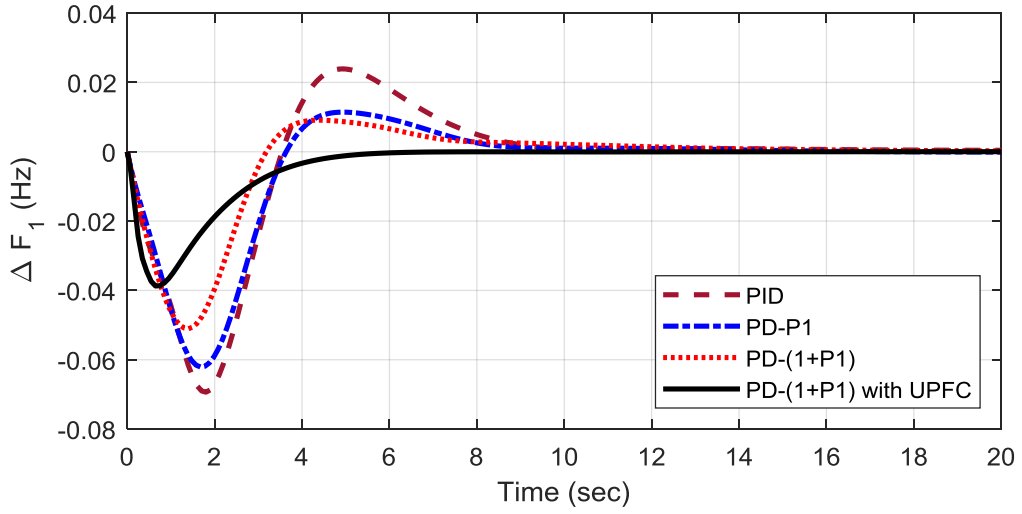

(a) ΔF_1

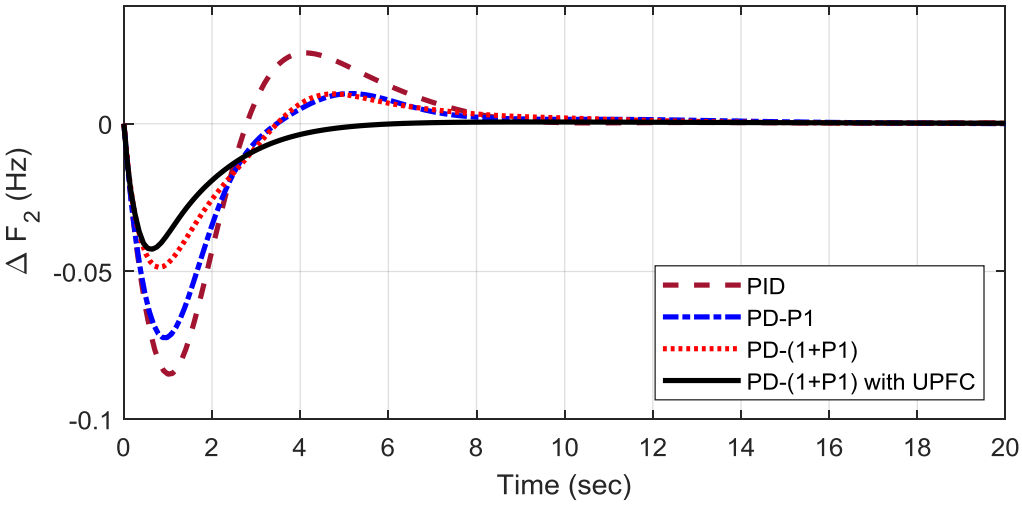

(b) ΔF_2

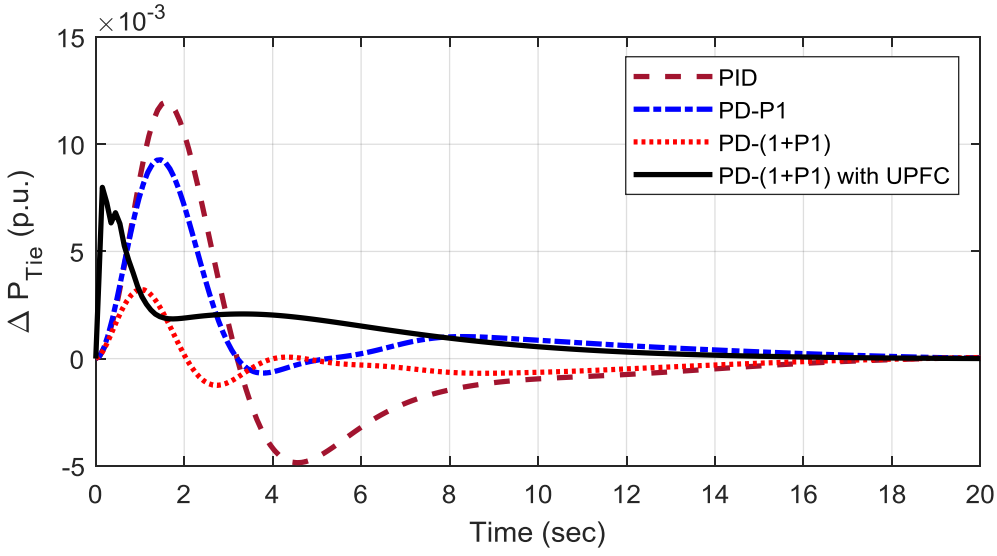

(c) ΔP_{Tie}

Fig. 6 System response for Case-1

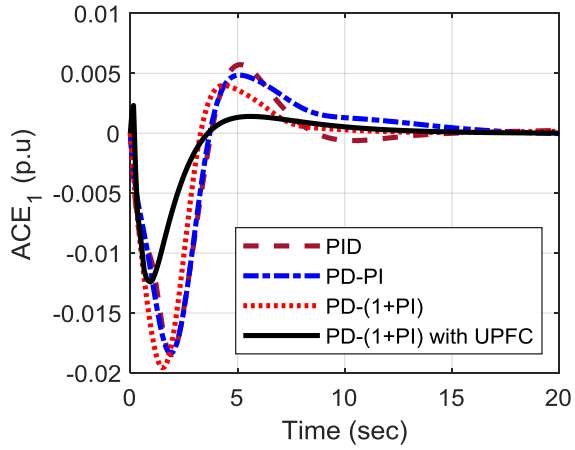
ACE1 (p.u)
Time (sec)
PID
PD-PI
PD-(1+PI)
PD-(1+PI) with UPFC

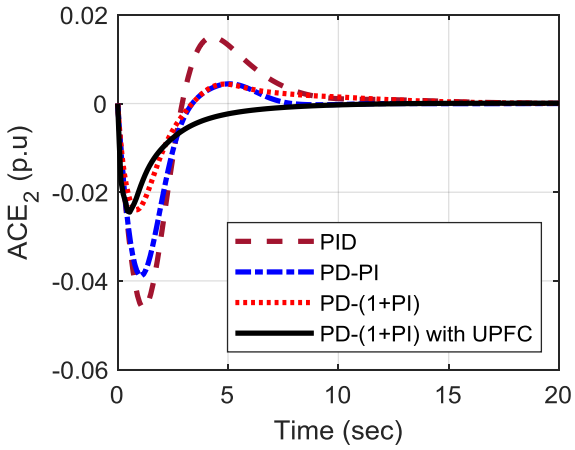
ACE2 (p.u)
Time (sec)
PID
PD-PI
PD-(1+PI)
PD-(1+PI) with UPFC

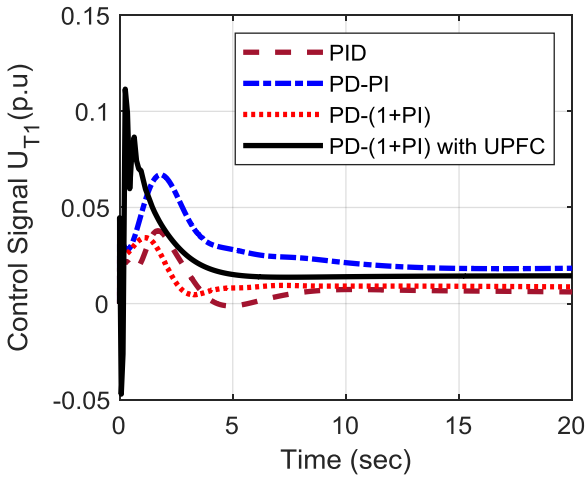
Control Signal UT1 (p.u)
Time (sec)
PID
PD-PI
PD-(1+PI)
PD-(1+PI) with UPFC

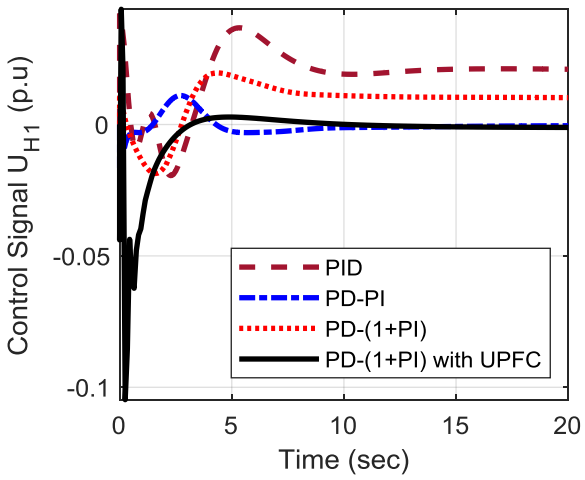
Control Signal UH1 (p.u)
Time (sec)
PID
PD-PI
PD-(1+PI)
PD-(1+PI) with UPFC

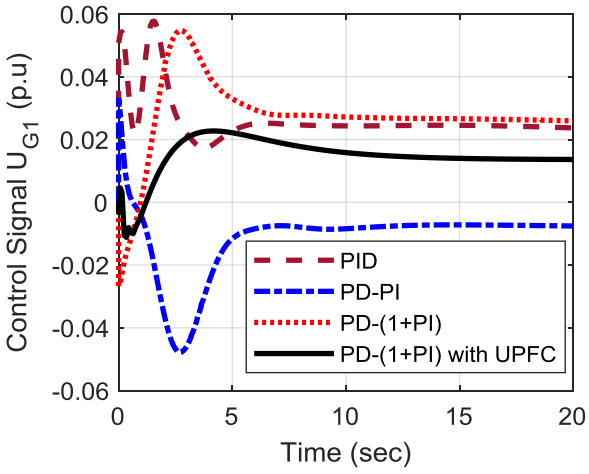
Control Signal UG1 (p.u)
Time (sec)
PID
PD-PI
PD-(1+PI)
PD-(1+PI) with UPFC

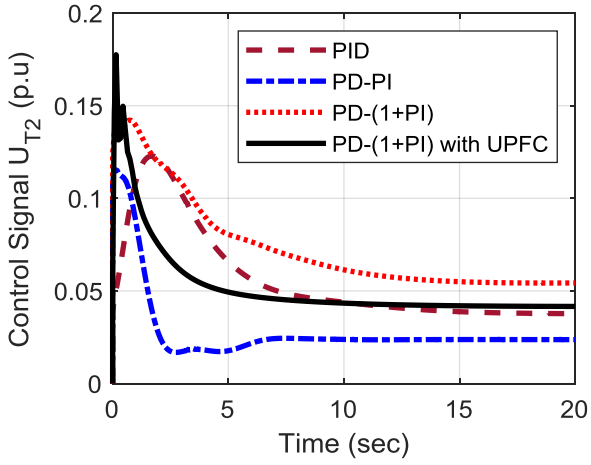
Control Signal UT2 (p.u)
Time (sec)
PID
PD-PI
PD-(1+PI)
PD-(1+PI) with UPFC

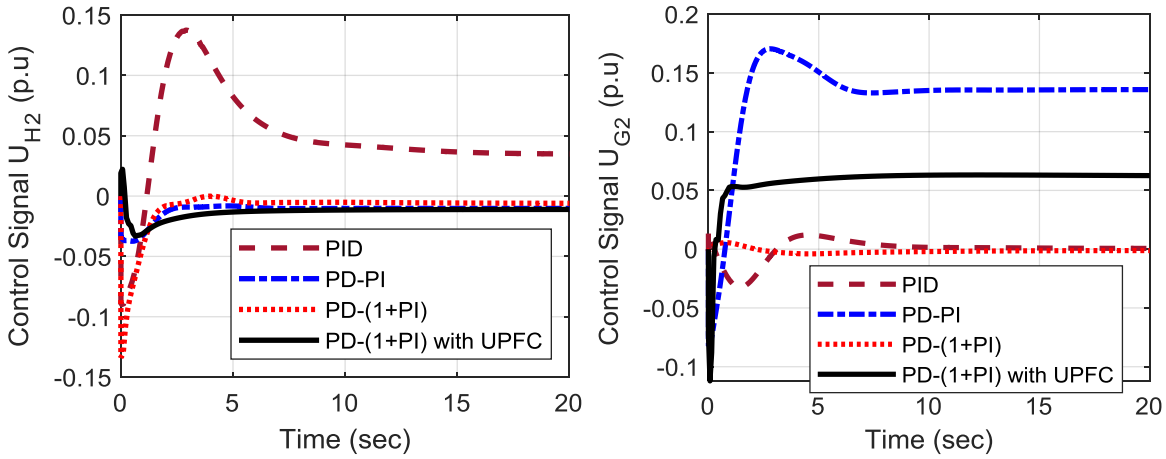

Fig. 7 Input and output control signals

Case 2:

At 20 seconds, the SLPs of area-1 are increased by 1 percent, whilst the SLPs of area-2 are decreased by 1.5 percent relative to Case-1. The dynamic responses of the IGOA-optimized PID, PD-PI, PD-(1+PI), and PD-(1+PI with UPFC are displayed in Figs. 8 (a)-(c), respectively. Figs. 8 (a)-(c) reveal that the transient performance of PD-(1+PI) controllers is superior to that of PID and PD-PI controllers in terms of low errors and MUs/MOs compared to the performance of other controllers. When UPFC is taken into account, performance improves even more.The assessment report of transient characteristics of various integral errors, maximum overshoot (MOs) and maximum undershoot (MUs), of ΔF_1, ΔF_2, ΔP_{Tie} of the suggested system for Case 2 is given in Table 7. This table demonstrates that the mathematical values *J*, integral errors, MOs, and MUs attributable to PD-(1+PI) with UPFC are the lowest when compared to alternative techniques. This can be seen by looking at the table. In comparison to PID and PD-PI, the suggested PD-(1+PI) method results in a decrease in *J* value of 80.05 percent, whereas PID and PD-PI each result in a reduction of 64.95 percent. When UPFC is accounted for in the system, the *J* value goes down by a certain percentage.

Table 7: Performance index comparison of IGOA optimized controllers for Case-2

Controller /Technique	J value	Integral errors					Max. Overshoots (MO_S)			Max. Undershoots (MU_s) (-ve)		
		ISE	ITAE	ITSE	IAE	ISTAE	ΔF_1	ΔF_2	ΔP_{Tie}	ΔF_1	ΔF_2	ΔP_{Tie}
PID	5.5899	0.0217	6.7293	0.0933	0.6965	138.4993	0.0239	0.0282	0.0120	0.0694	0.0848	0.0116
PD-PI	4.0706	0.0150	5.5189	0.0570	0.5388	122.2392	0.0114	0.0263	0.0093	0.0621	0.0724	0.0118
PD-(1+PI)	2.1984	0.0083	3.3186	0.0288	0.3832	65.5278	0.0091	0.0117	0.0032	0.0510	0.0486	0.0075
PD-(1+PI) with UPFC	1.2721	0.0046	2.0230	0.0097	0.2545	42.9832	0.0023	0.0081	0.0080	0.0387	0.0425	0.0094

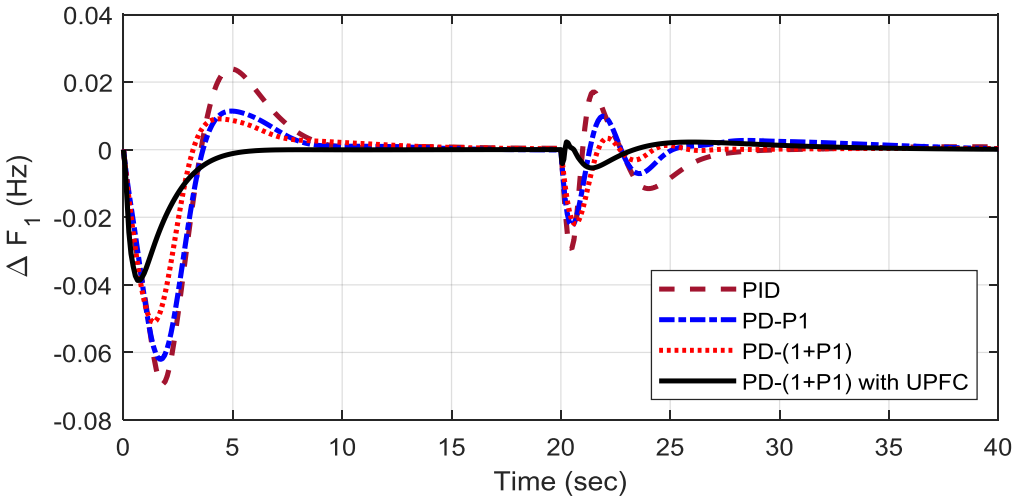

(a) ΔF_1

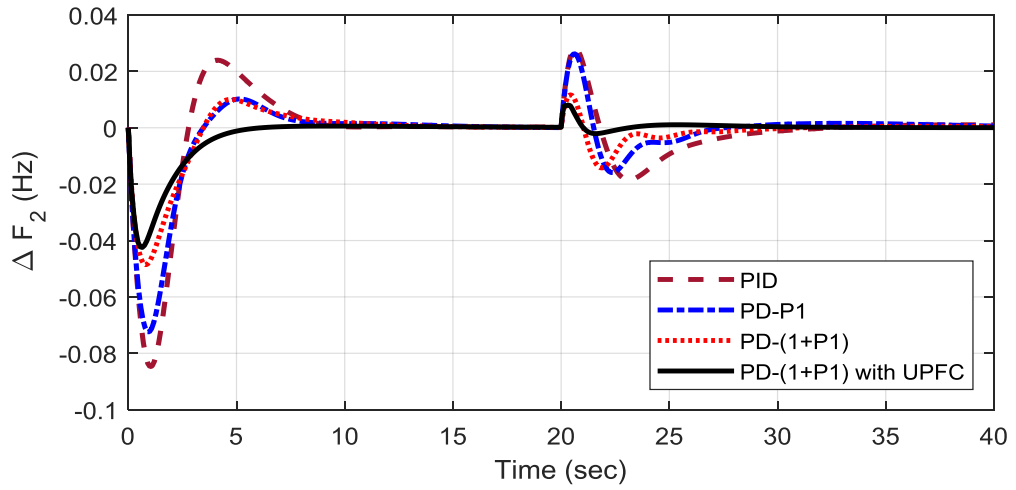

(b) ΔF_2

Fig. 8 System response for Case-2

Case 3:

When developing a system to work in the real world, it is likely that the predicted values of some of the system's parameters will be inaccurate. In addition, the values of the system parameters may change over the course of time, which would have a significant impact on how well the system would function. For this reason, it is essential to examine the performance of the system when the system parameters change. In this scenario, uncertainties in the system's characteristics are taken into account to demonstrate the adaptability and resilience of the proposed control method. For the purposes of sensitivity analysis, the system parameter (gains and temporal constants for all components) is modified by a 25 percent margin. Table 8 compiles the comparative report of transient features of different integral errors, *J* value, and change in *J* value for the aforementioned various scenarios. Figs. 9 and 10 provide the frequency deviations for +25 percent and -25 percent, respectively. It is evident from Table 8 and Figs. 9 and 10 that the PD-(1+PI) with UPFC method achieves the lowest *J* value and integral errors when compared to the other options that were taken into consideration. Fig. 11 shows MATLAB vs OPAL_RT results of the proposed model. Table. 9 shows the stability analysis results using system eigenvalues of the proposed model.

Table 8: Performance index comparison of IGOA optimized controllers for Case-3

Controller/ Technique	J value	Integral errors				
		ISE	ITAE	ITSE	IAE	ISTAE
+25%						
PID	4.7680	0.0183	6.6275	0.0774	0.6496	139.8521
PD-PI	3.6228	0.0130	4.5240	0.0414	0.4923	97.0246
PD-(1+PI) w/o UPFC	1.8683	0.0069	3.3648	0.0236	0.3588	69.1390
PD-(1+PI) with UPFC	1.2028	0.0042	2.3165	0.0097	0.2778	49.3053
-25%						
PID	6.8205	0.0267	6.9239	0.1295	0.7431	138.8649
PD-PI	5.1480	0.0196	7.2090	0.1078	0.6489	158.3879
PD-(1+PI) w/o UPFC	2.6026	0.0100	3.5996	0.0401	0.4085	71.2857
PD-(1+PI) with UPFC	1.3253	0.0048	1.8699	0.0102	0.2370	38.8395

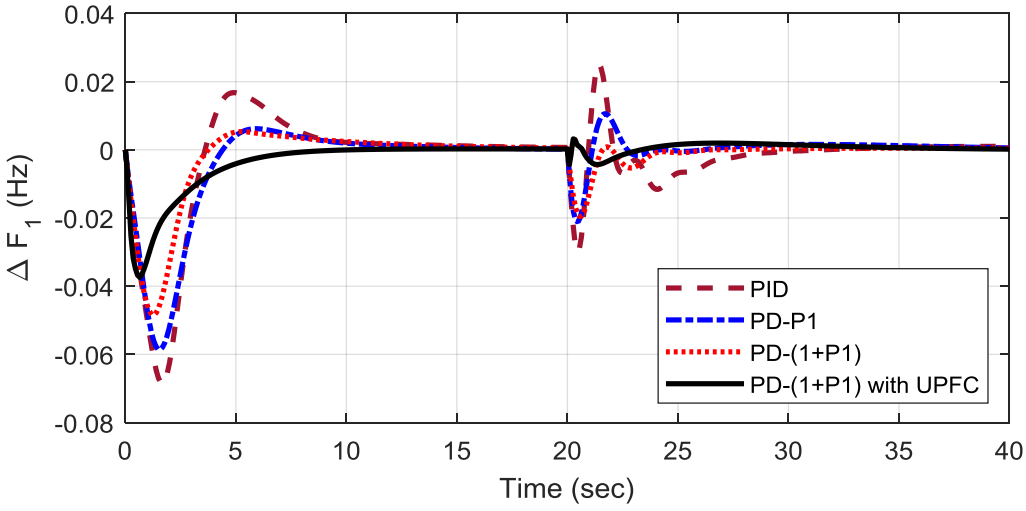

(a) ΔF_1

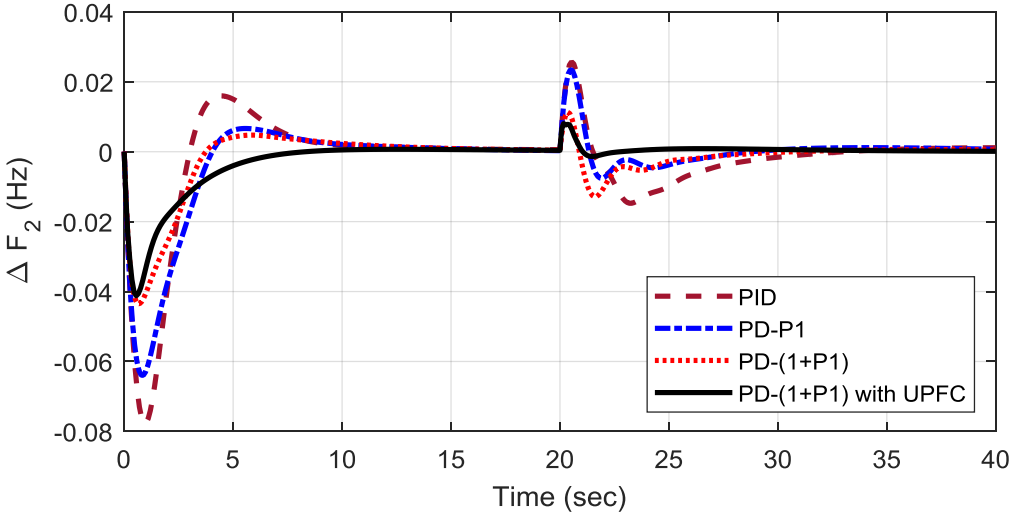

(b) ΔF_2

Fig. 9 System response for Case-3 (+25%)

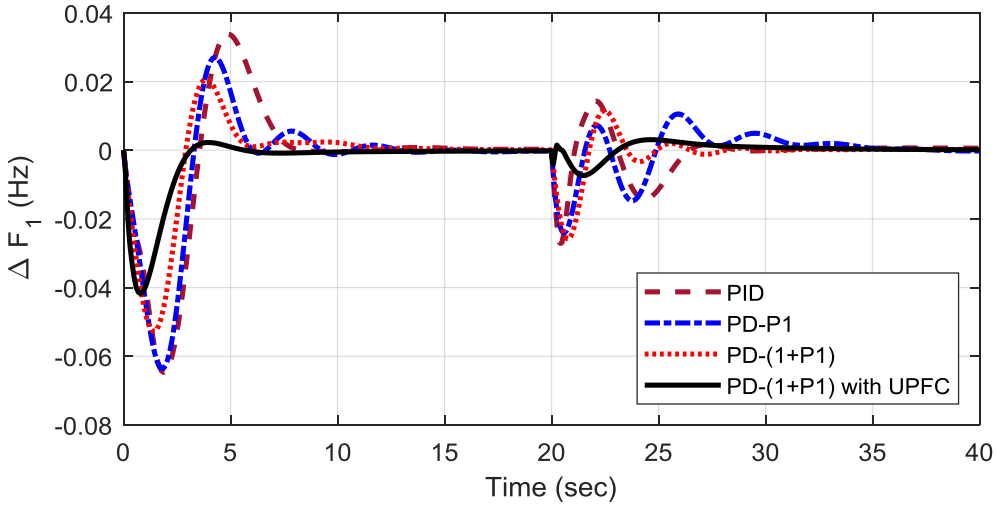

(a) ΔF_1

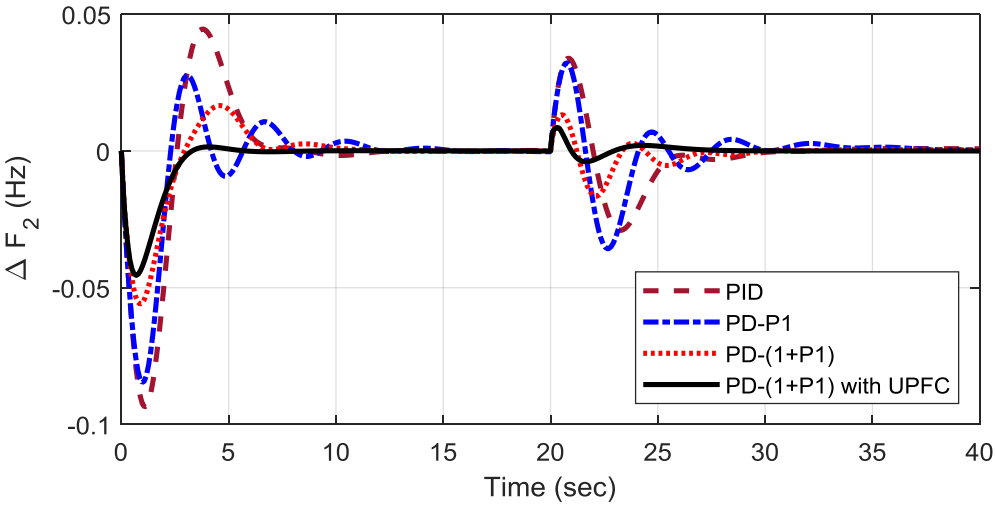

(b) ΔF_2

Fig. 10 System response for Case-3 (-25%)

Table 9: Stability analysis using system eigenvalues

PID	PD-PI	PD-(1+PI)	PD-(1+PI) with UPFC
-0.7626 ± 0.0231i	-0.9360 ± 0.1594i	-1.9213 ± 0.5481i	-5.8396 ± 9.7261i
-0.5570 ± 1.0221i	-0.5308 ±1.1760i	-0.5811 ± 1.1941i	-4.0531 ± 0.5164i
-0.2662 ± 2.4552i	-0.1759 ± 0.1901i	-0.2277 ± 0.1306i	-1.2645 ± 2.4473i
-0.2164 ± 0.1047i	-0.0905 ± 2.4079i	-0.1626 ± 2.4679i	-0.6435 ± 0.3557i
			-0.1729 ± 0.0430i

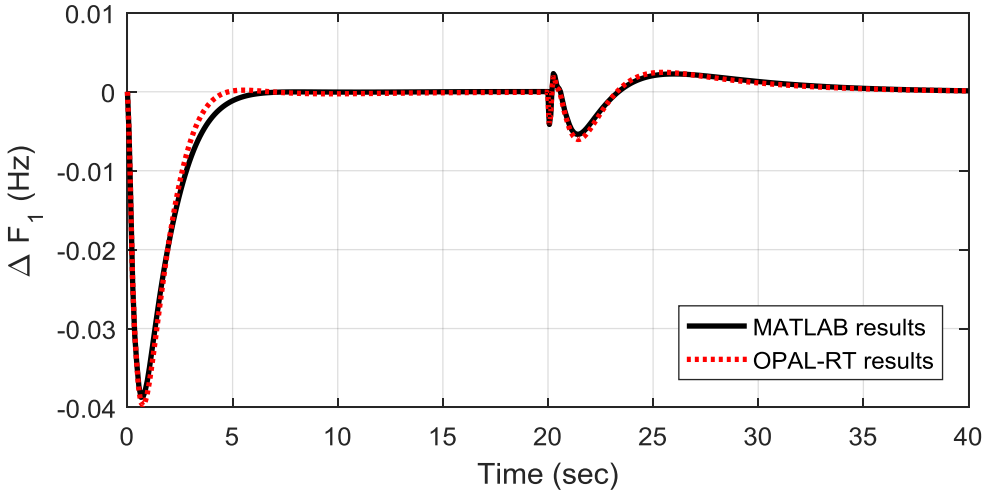

(a) ΔF_1

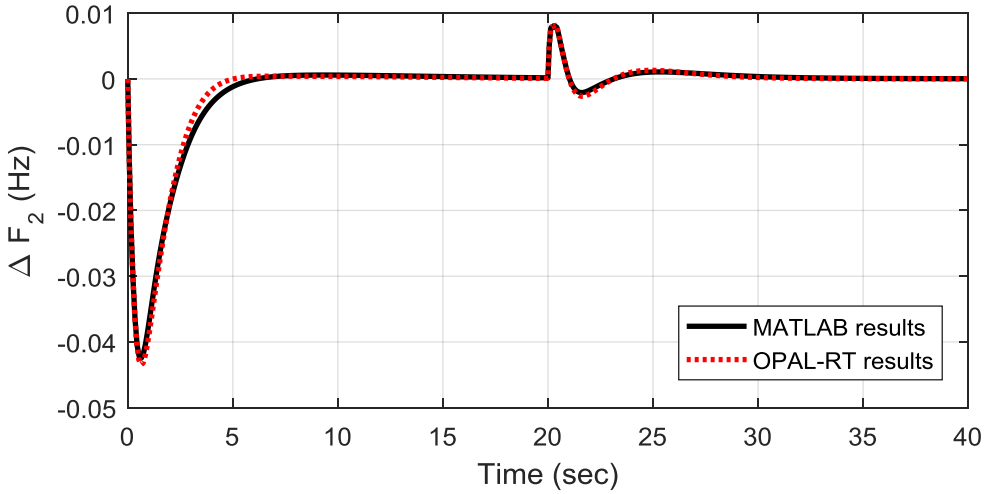

(b) ΔF_2

Fig. 11 MATLAB vs OPAL_RT results

It is worth mentioning here that an offline optimization algorithm has been employed in this study to tune a controller based on simulation data that is based on the system model. This optimization is not usable in online experimental study without modeling and simulating the controller iteratively. However, as the controllers are designed before it is put into action, offline optimization can be applied to tune the controller parameters.

6. Conclusion

Using an enhanced GOA (IGOA), this study proposes a new method for determining PD-(1+PI) controller parameters for frequency regulation of Automatic Generation (AGC) management of power systems with UPFC. Initially, the suggested IGOA approach is used for the design of PID controllers, and the results are compared to those of the GA, PSO, and GOA procedures. It is found that the suggested IGOA approach reduces J value by 45.55 percent compared to GA, 34.38 percent compared to PSO, and 23.77 percent compared to GOA. In the subsequent phase, PD-PI, PD-(1+PI), and PD-(1+PI) with UPFC are taken into account. It has been found that the

recommended PD-(1+PI) decreases the J value by 60.37 percent for comparable step load perturbations in each location, while the PD-PI and PID lower the J value by 45.16 percent and 45.37 percent, respectively. When UPFC is used, the J value is reduced by an additional 40.36 percent when compared to when it is not used. The performance of the system with multiple SLPs and under parameter variation conditions is also investigated. It has been observed that the suggested method for controlling frequency is reliable and carries out its duties adequately even in the face of parameter uncertainty in the range of 25 percent. Lastly, this obtained results can be applied to recent nature based optimization techniques such as Artificial Gorilla Troops Optimizer, Aquila Optimizer, Leader Harris Hawks optimization, Dingo Optimization Algorithm (DOA) and so on with different scenarios.

7. Competing Interests

The authors state that there were no commercial or financial interactions that might be considered as a possible conflict of interest during the research's conduct.

8. Funding

This research is not sponsored monetarily.

9. Ethical acceptance

None of the authors of this article have undertaken human or animal research.

10. Knowledgeable consent

Each participant in the research supplied their informed consent willingly.

11. References

Abd-Elazim SM and Ali ES (2016) Load frequency controller design via BAT algorithm for nonlinear interconnected power system. *International Journal of Electrical Power & Energy Systems*, 77: 166-177. https://doi.org/10.1016/j.ijepes.2015.11.029

Abou El-Ela AA, El-Sehiemy RA, Shaheen AM and Diab AEG (2022) Design of cascaded controller based on coyote optimizer for load frequency control in multi-area power systems with renewable sources. *Control Engineering Practice*, 121: 105058. https://doi.org/10.1016/j.conengprac.2021.105058

Barisal AK (2015) Comparative performance analysis of teaching learning based optimization for automatic load frequency control of multi-source power systems. *International Journal of Electrical Power & Energy Systems*, 66: 67-77. https://doi.org/10.1016/j.ijepes.2014.10.019

Dash P, Saikia LC and Sinha N (2014) Comparison of performances of several Cuckoo search algorithm based 2DOF controllers in AGC of multi-area thermal system. *International Journal of Electrical Power & Energy Systems*, 55: 429-436. https://doi.org/10.1016/j.ijepes.2013.09.034

Dash P, Saikia LC and Sinha N (2015) Automatic generation control of multi area thermal system using Bat algorithm optimized PD–PID cascade controller. *International Journal of Electrical Power & Energy Systems*, 68: 364-372. https://doi.org/10.1016/j.ijepes.2014.12.063

Dash P, Saikia LC and Sinha N (2016) Flower pollination algorithm optimized PI-PD cascade controller in automatic generation control of a multi-area power system. *International Journal of Electrical Power & Energy Systems*, 82: 19-28. https://doi.org/10.1016/j.ijepes.2016.02.028

Eftimie R, De Vries G, Lewis MA and Lutscher F (2007) Modeling group formation and activity patterns in self-organizing collectives of individuals. *Bulletin of mathematical biology*, 69(5): 1537-1565. https://doi.org/10.1007/s11538-006-9175-8

Elgerd OI (1971) *Fundamental Concepts of Electric Energy Systems Engineering, Electric Energy Systems Theory: An Introduction*, 1st ed. New Delhi: Tata McGraw-Hill, pp.11-43. https://catedras.facet.unt.edu.ar/sep/wp-content/uploads/sites/20/2020/03/Electric-Energy-Systems-Theory-An-Introduction-Elgerd.pdf

Ezzat D, Hassanien AE, Darwish A, Yahia M, Ahmed A and Abdelghafar S (2021) Multi-objective hybrid artificial intelligence approach for fault diagnosis of aerospace systems. *IEEE Access*, 9: 41717-41730. https://doi.org/10.1109/ACCESS.2021.3064976

Fosha CE and Elgerd OI (1970) The megawatt-frequency control problem: A new approach via optimal control theory. *IEEE Transactions on Power Apparatus and Systems*, (4): 563-577. https://doi.org/10.1109/TPAS.1970.292603

Guha D, Roy PK and Banerjee S (2022) Quasi-oppositional JAYA optimized 2-degree-of-freedom PID controller for load-frequency control of interconnected power systems. *International Journal of Modelling and Simulation*, 42(1): 63-85. https://doi.org/10.1080/02286203.2020.1829444

Irudayaraj AXR, Wahab NIA, Premkumar M, Radzi MAM, Sulaiman NB, Veerasamy V, Farade RA and Islam MZ (2022) Renewable sources-based automatic load frequency control of interconnected systems using chaotic atom search optimization. *Applied Soft Computing*, 119: 108574. https://doi.org/10.1016/j.asoc.2022.108574

Jiang Y, Gao W, Na J, Zhang D, Hämäläinen TT, Stojanovic V and Lewis FL (2022) Value iteration and adaptive optimal output regulation with assured convergence rate. *Control Engineering Practice*, 121: 105042. https://doi.org/10.1016/j.conengprac.2021.105042

Kaliannan J, Baskaran A, Dey N, Ashour AS and Kumar R (2019) Bat algorithm optimized controller for automatic generation control of interconnected thermal power system. *In Information Technology and Intelligent Transportation Systems*, pp. 276-286. IOS Press. https://doi.org/10.3233/978-1-61499-939-3-276

Khokhar B, Dahiya S and Parmar KS (2021) Load frequency control of a microgrid employing a 2D Sine Logistic map based chaotic sine cosine algorithm. *Applied Soft Computing*, 109: 107564. https://doi.org/10.1016/j.asoc.2021.107564

Khuntia SR and Panda S (2012) Simulation study for automatic generation control of a multi-area power system by ANFIS approach. *Applied soft computing*, 12(1): 333-341. https://doi.org/10.1016/j.asoc.2011.08.039

Kundur PS and Malik OP (2022) *Power system stability and control*. McGraw-Hill Education. http://powerunit-ju.com/wp-content/uploads/2018/01/Power-System-Stability-and-Control-by-Prabha-Kundur.pdf

Mohanty B, Panda S and Hota PK (2014) Controller parameters tuning of differential evolution algorithm and its application to load frequency control of multi-source power system. *International journal of electrical power & energy systems*, 54: 77-85. https://doi.org/10.1016/j.ijepes.2013.06.029

Mohanty D and Panda S (2021) A modified moth flame optimisation technique tuned adaptive fuzzy logic PID controller for frequency regulation of an autonomous power system. *International Journal of Sustainable Energy*, 40(1): 41-68. https://doi.org/10.1080/14786451.2020.1787412

Naidu K, Mokhlis H and Bakar AA (2014) Multiobjective optimization using weighted sum artificial bee colony algorithm for load frequency control. *International Journal of Electrical Power & Energy Systems*, 55: 657-667. https://doi.org/10.1016/j.ijepes.2013.10.022

Narain G, Hingorani and Gyugyi L (2000) *Understanding FACTS: concepts and technology of flexible AC transmission systems*. Wiley-IEEE Press. https://ieeexplore.ieee.org/servlet/opac?bknumber=5264253

Nayak PC, Prusty UC, Prusty RC and Barisal AK (2018), March. Application of SOS in fuzzy based PID controller for AGC of multi-area power system. *In 2018 Technologies for Smart-City Energy Security and Power (ICSESP)*, pp. 1-6. IEEE. https://doi.org/10.1109/ICSESP.2018.8376709

Nayak PC, Sahoo A, Balabantaraya R and Prusty RC (2018), March. Comparative study of SOS & PSO for fuzzy based PID controller in AGC in an integrated power system. *In 2018 Technologies for Smart-City Energy Security and Power (ICSESP)*, pp. 1-6. IEEE. https://doi.org/10.1109/ICSESP.2018.8376700

Nedić N, Pršić D, Fragassa C, Stojanović V and Pavlovic A (2017) Simulation of hydraulic check valve for forestry equipment. *International journal of heavy vehicle systems*, 24(3): 260-276. https://doi.org/10.1504/IJHVS.2017.084875

Padhan S, Sahu RK and Panda S (2014) Application of firefly algorithm for load frequency control of multi-area interconnected power system. *Electric power components and systems*, 42(13): 1419-1430. https://doi.org/10.1080/15325008.2014.933372

Padhy S and Panda S (2021) Application of a simplified Grey Wolf optimization technique for adaptive fuzzy PID controller design for frequency regulation of a distributed power generation system. *Protection and Control of Modern Power Systems*, 6(1): 1-16. https://doi.org/10.1186/s41601-021-00180-4

Peddakapu K, Mohamed MR, Srinivasarao P and Leung PK (2021) Frequency stabilization in interconnected power system using bat and harmony search algorithm with coordinated controllers. *Applied Soft Computing*, 113: 107986. https://doi.org/10.1016/j.asoc.2021.107986

Prasad B, Prasad CD and Kumar GP (2015) Effect of load parameters variation on AGC of two area thermal power system in the presence of integral and PSO-PID controllers. *i-Manager's Journal on Instrumentation & Control Engineering*, 3(2): 16. https://doi.org/10.1109/PCCCTSG.2015.7503944

Sahu PC, Prusty RC and Panda S (2019) A gray wolf optimized FPD plus (1+ PI) multistage controller for AGC of multisource non-linear power system. *World Journal of Engineering*, 16(1): 1-13. https://doi.org/10.1108/WJE-05-2018-0154

Sahu PC, Prusty RC and Panda S (2021) Improved-GWO designed FO based type-II fuzzy controller for frequency awareness of an AC microgrid under plug in electric vehicle. *Journal of Ambient Intelligence and Humanized Computing*, 12(2): 1879-1896. https://doi.org/10.1007/s12652-020-02260-z

Sahu PR, Hota PK and Panda S (2018) Power system stability enhancement by fractional order multi input SSSC based controller employing whale optimization algorithm. *Journal of Electrical Systems and Information Technology*, 5(3): 326-336. https://doi.org/10.1016/j.jesit.2018.02.008

Sahu RK, Sekhar GC and Panda S (2015) DE optimized fuzzy PID controller with derivative filter for LFC of multi source power system in deregulated environment. *Ain Shams Engineering Journal*, 6(2): 511-530. https://doi.org/10.1016/j.asej.2014.12.009

Sahu RK, Panda S and Rout UK (2013) DE optimized parallel 2-DOF PID controller for load frequency control of power system with governor dead-band nonlinearity. *International Journal of Electrical Power & Energy Systems*, 49: 19-33. https://doi.org/10.1016/j.ijepes.2012.12.009

Sahu RK, Panda S and Sekhar GC (2015) A novel hybrid PSO-PS optimized fuzzy PI controller for AGC in multi area interconnected power systems. *International Journal of Electrical Power & Energy Systems*, 64: 880-893. https://doi.org/10.1016/j.ijepes.2014.08.021

Saremi S, Mirjalili S and Lewis A (2017) Grasshopper optimisation algorithm: theory and application. *Advances in engineering software*, 105: 30-47. https://doi.org/10.1016/j.advengsoft.2017.01.004

Shayeghi H, Rahnama A and Alhelou HH (2021) Frequency control of fully-renewable interconnected microgrid using fuzzy cascade controller with demand response program considering. *Energy Reports*, 7: 6077-6094. https://doi.org/10.1016/j.egyr.2021.09.027

Sulaiman M, Masihullah M, Hussain Z, Ahmad S, Mashwani WK, Jan MA and Khanum RA (2019) Implementation of improved grasshopper optimization algorithm to solve economic load dispatch problems. *Hacettepe Journal of Mathematics and Statistics*, 48(5): 1570-1589. https://doi.org/10.15672/hujms.507579

Zhou L, Tao H, Paszke W, Stojanovic V and Yang H (2020) PD-type iterative learning control for uncertain spatially interconnected systems. *Mathematics*, 8(9): 1528. https://doi.org/10.3390/math8091528